

Jensen-Shannon Complexity and Permutation Entropy Analysis of Geomagnetic Auroral Currents

Adnane Osmane¹ , Andrew P. Dimmock², and Tuija I. Pulkkinen^{3,4} 

¹Department of Physics, University of Helsinki, Helsinki, Finland, ²IRF Swedish Institute of Space Physics, Uppsala, Sweden, ³Department of Climate and Space Sciences, University of Michigan, Ann Arbor, MI, USA, ⁴School of Electrical Engineering, Aalto University, Espoo, Finland

Key Points:

- Jensen-Shannon complexity plane is used for first time to analyze auroral geomagnetic indices
- Auroral indices are shown to be inconsistent with low-dimensional chaotic processes
- Maximum in complexity occurs on time scales ranging between 10 and 40 min

Correspondence to:

A. Osmane,
adnane.osmane@helsinki.fi

Citation:

Osmane, A., Dimmock, A. P., & Pulkkinen, T. I. (2019). Jensen-Shannon complexity and permutation entropy analysis of geomagnetic auroral currents. *Journal of Geophysical Research: Space Physics*, 124, 2541–2551. <https://doi.org/10.1029/2018JA026248>

Received 29 OCT 2018

Accepted 14 MAR 2019

Accepted article online 18 MAR 2019

Published online 5 APR 2019

Abstract In this study we determine whether auroral westward currents can be characterized by low-dimensional chaotic attractors through the use of the complexity-entropy methodology developed by Rosso et al. (2007, <https://doi.org/10.1103/PhysRevLett.99.154102>) and based on the permutation entropy developed by Bandt and Pompe (2002, <https://doi.org/10.1103/PhysRevLett.88.174102>). Our results indicate that geomagnetic auroral indices are indistinguishable from stochastic processes from time scales ranging from a few minutes to 10 hr and for embedded dimensions $d < 8$. Our results are *inconsistent* with earlier studies of Baker et al. (1990, <https://doi.org/10.1029/GL017i001p00041>), Pavlos et al. (1992), D. Roberts et al. (1991, <https://doi.org/10.1029/91GL00021>), D. A. Roberts (1991, <https://doi.org/10.1029/91JA01088>), and Vassiliadis et al. (1990, <https://doi.org/10.1029/GL017i011p01841>, 1991, <https://doi.org/10.1029/91GL01378>) indicating that auroral geomagnetic indices could be reduced to low-dimensional systems with chaotic dynamics.

1. Introduction

The discovery 50 years ago that fully developed turbulence could in principle be the result of only three instabilities (Ruelle & Takens, 1971), rather than an infinite number (Landau, 1944), together with the experimental confirmation by Gollub and Swinney (1975) that universal behavior described by a few parameters could be observed in a fluid system, has led to what some authors described as a “chaos revolution” (Lovejoy & Schertzer, 1998). The realization that nonlinear systems with a very large number of degrees of freedom could be described by low-dimensional dynamical systems naturally found a promising niche in a wide range of space plasma research, and especially in space weather studies, in order to alleviate the computational cost of modeling the Earth’s magnetosphere. Following the development of empirical techniques for detecting deterministic chaos by Grassberger and Procaccia (1983), a plethora of studies (Baker et al., 1990; Pavlos et al., 1992; D. A. Roberts, 1991; A. Roberts et al., 1991; Vassiliadis et al., 1990; Vassiliadis et al., 1991) using geomagnetic indices argued that the Earth’s magnetospheric dynamics could be reduced to a low-dimensional dynamical system. However, it was first shown by Osborne and Provenzale (1989) for a general case, and later by Prichard and Price (1992) and Shan et al. (1991) for space weather studies, that the empirical technique could not differentiate between colored noise and deterministic chaos in geomagnetic time series, due to long autocorrelation times inherent to the former.

Nonetheless, the ideas provided by deterministic chaos were extended to nonlinear stochastic systems by the use of self-organized critical (SOC) models, which is cellular automata defined by a certain class of discontinuous rules and appropriate boundary conditions (Lovejoy & Schertzer, 1998). SOC systems were shown to evolve spontaneously to critical states describable by a low-dimensional dynamical system (Chang, 1992). Consequently, Pulkkinen et al. (2006), Balasis et al. (2006), Consolini and Marcucci (1997), Dobias and Wanliss (2009), Klimas et al. (1996), Klimas et al. (2000), Uritsky and Pudovkin (1998), Uritsky et al. (2001), Uritsky et al. (2006), Valdivia et al. (2003), Wanliss et al. (2005), and Wanliss and Dobias (2007) extended these ideas to magnetospheric systems, demonstrating that nonlinear stochastic models were a better representation than low-dimensional chaotic attractors. The emergence of dynamical correlations and non-Markovian features during intense geomagnetic storms, analogous to the emergence of long-range coherence in out-of-equilibrium systems, implied a reduction in the number of degrees of freedom of the system and inherent nonlinearities (Consolini & De Michelis, 2014).

In this study, we contribute to the decades-old discussions on the properties of geomagnetic processes by using permutation entropy, a measure developed by Bandt and Pompe (2002), to quantify complexity in measured time series. Whereas common measures of complexity, such as the Kolmogorov-Sinai entropy, or the Shannon entropy, ignore temporal order of the values in the time series, entropy measures of ordinal patterns preserve information of temporal order and provides for an alternative measure of complexity (Riedl et al., 2013). Permutation entropy has now been tested across several scientific disciplines and is now being used to characterize processes in laboratory and geophysical plasma experiments (Consolini & De Michelis, 2014; Maggs & Morales, 2013; Weck et al., 2015).

For example, using the complexity-entropy measure developed by Rosso et al. (2007), Weck et al. (2015) demonstrate that solar wind turbulent fluctuations are stochastic, rather than chaotic. In the context of geomagnetic activity, it is of primary interest to determine whether, and under which time scales, geomagnetic currents demonstrate signatures of low-dimensional dynamical systems, if any. Using the methodology developed by Rosso et al. (2007), we hereafter revisit the question as to whether auroral geomagnetic indices can be characterized as a low-dimensional chaotic attractor and use for the first time the Jensen-Shannon complexity on auroral geomagnetic indices. In section 2 we describe the data set and the complexity-entropy plane used for distinguishing between stochastic and chaotic time series. In section 3 we present the results. In sections 4 and 5 we discuss our findings, their relation to previous studies, and trace out a plan for future studies.

2. Methodology

2.1. Data Sets

The data are obtained from the OMNI database (<http://omniweb.gsfc.nasa.gov>), which provides estimates of solar wind parameters at the bow shock nose (Farris & Russell, 1994) by propagating observations performed by several spacecraft further upstream (King & Papitashvili, 2005) as well as measures of geomagnetic activity. We focus primarily on the *AL* index, which is notoriously difficult to predict Newell et al. (2007), presumably because of inherent nonlinearities in its dynamics.

AL provides an estimate of the maximum westward electrojet intensity using 12 magnetometer stations around the northern auroral region (Berthelier & Menvielle, 1993). Outside of substorm intervals, *AL* can be thought of as a measure of convection, while during substorms the largest deviations in the horizontal component typically originate from the substorm current wedge. By nature, *AL* is therefore highly asymmetric and peaks at low values, reflecting quiet time convection effects and heavy tails associated with substorm occurrences (Newell et al., 2007; Tanskanen et al., 2002).

2.2. Permutation Entropy

Permutation entropy was proposed by Bandt and Pompe (2002) as a complexity measure for arbitrary time series, that is, stationary or nonstationary, deterministic or stochastic, and periodical or noisy. However, it should be pointed that a weak form of stationary assumption is required; that is, for $s < d$, the probability for $x_t < x_{t+s}$ should not depend on t (Rosso et al., 2013). The Bandt-Pompe permutation entropy is computed on the basis of a probability distribution quantifying the rate of occurrence of *amplitude orderings* in a time signal $\mathcal{T}(t) \equiv \{x_t; t = 1, \dots, N\}$ measured at N evenly spaced discrete points. Computation of the probability is done for an embedding space of dimension d , which translates in determining patterns of length d in the order in which they appear in the time series. (For readers not familiar with the idea of an embedding dimension and delay we recommend the book by Ott, 2002, Section 3.8.) The d values are called *d tuples*. For instance, for $d = 3$, a number of $d! = 6$ possible sequences are possible, that is, (1,2,3), (1,3,2), (2,1,3), (2,3,1), (3,1,2), and (3,2,1). For a signal with N elements, the relative frequency of each of the possible sequences is computed for three successive values of the time series. The number of successive values for embedding dimension d and signal of N elements consists in $1 \leq n \leq N - d + 1$ distinct d tuples ordered as $t_j, t_{j+1} \dots t_{j+d-1}$. Similarly, for the embedding dimension chosen in our analysis, that is, $d = 6$, a signal with $N = 10,000$ elements has $1 \leq n \leq N - d + 1 = 9,995$ distinct d tuples $t_j, t_{j+1} \dots t_{j+5}$, or ordinal patterns. Within each d tuple, an ordering of the amplitude is obtained as a function of the $d!$ possible permutations, for example, 720 permutations for $d = 6$. The permutation entropy is then computed for a particular signal by computing the frequency of occurrence of each possible permutations of the amplitude

ordering. For a set of probabilities P , of dimension $d!$ and probability of occurrence $p_j \geq 0; j = 1, 2, \dots, d!$, the permutation entropy is defined in terms of the Shannon entropy, S , as

$$S(P) = - \sum_{j=1}^{d!} p_j \log(p_j). \quad (1)$$

In the following we use the normalized Shannon entropy, H , defined as

$$H(P) = S(P) / \log(d!) = S(P) / P_e, \quad (2)$$

and the Shannon entropy per symbol, h_n , defined as

$$h_n(P) = \frac{S(P)}{d-1}. \quad (3)$$

The denominator in the equation of $H(P)$ is the maximum Shannon entropy obtained when all states have equal probabilities; that is, $p_j = 1/d!; \forall j$ and this maximum probability is here denoted as P_e . The fundamental underlying idea behind the Bandt-Pompe permutation entropy is that some ordinal patterns may be forbidden, whereas others may be favored, making the information content less random than in stochastic systems. In theory, one might therefore be able to differentiate stochastic and deterministic fluctuations through the use of the permutation entropy.

However, as with all mathematical tools, one has to be aware of the advantages and limitations. In terms of advantages, the permutation entropy incorporates temporal order and is computationally very fast (Riedl et al., 2013). Additionally, it is invariant under any monotonic transformation of the time series; for example, scaling the data has no effect on the resulting distribution of permutation patterns. A consequence of the latter property is that the permutation entropy does not preserve information of the amplitude in the ordinal patterns. But more importantly, finite time series constrain the choice of the embedding dimension d . Since the number of possible amplitude permutations increases rapidly as $d!$, the value of d must be chosen such that $N \gg d!$; that is, the number of points in our time series must be sufficiently large for us to sample the relative distribution of each $d!$ permutations. In our case, we use $d = 6$ for time series with $N = 43,200$ points, corresponding to 30 days of 1-min sampling. The maximum embedded delay corresponds to $\tau = 600$ min, and the minimum number of segments corresponds to $N - (d-1)\tau > 40,000$. (Applying our analysis to delays ranging from days to months none of the conclusions presented hereafter were modified. However, it was not possible to test the methodology for time scales ranging from years to solar cycle periods due to data gaps.) Hence, we use more than 40,000 segments to distinguish the frequency of $d! = 720$ patterns. Consequently, for a given collection of d tuples, the size in time of the structures, or patterns, investigated is $d\Delta t$, where Δt is the sampling time. In order to study structures with size $d\Delta t \geq 10$, it is often not practically possible to increase the embedding dimension beyond $d = 7$ since $8! = 40,320$ and one must keep in mind the requirement that $N \gg d!$. In case of auroral indices, setting an embedding dimension of 8 would require a time series of length $N > 4 \cdot 10^6$ and corresponding to 280 days of 1-min sampled data. Large structures can nonetheless still be investigated by adding an additional parameter τ to subsample the time series. In the subsampled signal the interval between successive data point is $d\tau$ rather Δt . This technique naturally reduces the Nyquist frequency and the number of points to N/τ but preserves the total time of the signal (Maggs & Morales, 2013; Weck et al., 2015). For an embedding dimension $d > 2$ and embedded delay τ , a time series with N points contains $N - (d-1)\tau$ segments upon which the $d!$ permutations are computed. Once again, one needs to be very careful in selecting a sufficiently large number of points to make sure that all possible permutations can be accounted for. If one only has 1,000 segments available to sample the relative occurrence of 720 permutations, it is highly unlikely that even if the time series is stochastic, all possible permutations would be appropriately sampled. One might therefore conclude, incorrectly, that some patterns are forbidden and that the resulting entropy might be indicative of a deterministic time series. The time series length must be sufficiently large in order for all permutation patterns to be measured and thereby confirm the deterministic properties of the time series. This last constraint is particularly important when studying colored noise with very long autocorrelation times (Takalo et al., 1994). The permutation entropy analysis can be rendered useless if N is not sufficiently large, and one is therefore forced to seek alternative approaches to differentiate stochastic from deterministic fluctuations.

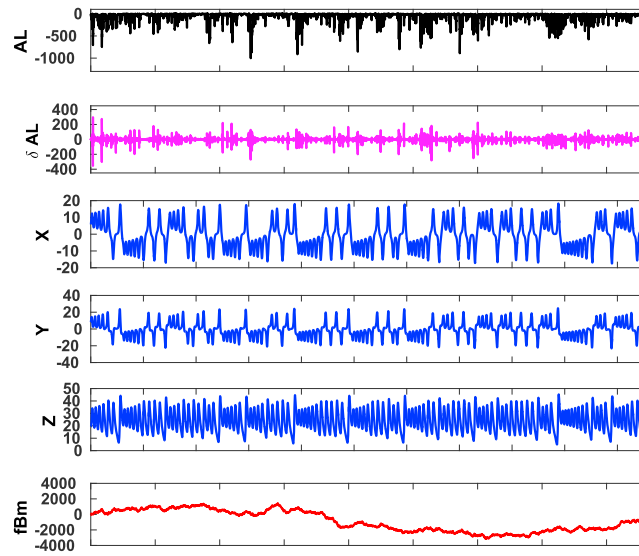


Figure 1. Top two panels show AL and $\delta AL = AL_{i+1} - AL_i$ time series for an interval of 4 months spanning 1 January to 30 April 2009. The panels with blue traces show time series for the Lorenz attractor with parameters $a = 10$, $b = 8/3$, and $c = 28$. The bottom panel shows an example of fractional Brownian motion with Hurst exponent $h_u = 0.8$.

2.3. Jensen-Shannon Complexity

A solution to supersede this last limitation of the permutation entropy and a means to distinguish between long correlated noise and deterministic time series was outlined by Rosso et al. (2007). Using Shannon's formulation of entropy for ordinal patterns and the Jensen-Shannon complexity as a measure of statistical complexity, Rosso et al. (2007) have shown that despite common properties (wideband power spectrum, irregular behavior of measured signals) it is after all possible to distinguish between stochastic and chaotic signals from their location in terms of an entropy-complexity plane. Hence, Rosso et al. (2007) combine the complexity measure of Bandt and Pompe and the Jensen-Shannon complexity, here defined as

$$C_j^S = D(P) \times H(P) = -2 \frac{S\left(\frac{P+P_e}{2}\right) - \frac{1}{2}S(P) - \frac{1}{2}S(P_e)}{\frac{d^{l+1}}{d!} \log(d! + 1) - 2 \log(2d!) + \log(d!)} H(P). \quad (4)$$

This complexity measure is the product of the normalized Shannon entropy, $H(P)$, and the Jensen divergence:

$$D(P) = S\left(\frac{P+P_e}{2}\right) - \frac{1}{2}S(P) - \frac{1}{2}S(P_e), \quad (5)$$

hence the Jensen-Shannon denominator. The argument in the denominator serves as normalization constant for the Jensen divergence. The divergence can be interpreted as the distance between our distribution of ordinal patterns and the distribution that maximizes the Shannon distribution, that is, P_e defined above. It is easy to see that it takes the value of 0 when $P = P_e$, that is, when all ordinal patterns are equally likely the Jensen-Shannon complexity is 0. Built from the square of the Shannon entropy, it has a parabolic shape when plotted against the permutation entropy, but more crucially, the Jensen-Shannon complexity can hold multiple values for a fixed Shannon entropy. It is this particular property that allows one to distinguish stochastic noise with long autocorrelation times to deterministic and chaotic fluctuations. Thus, a fixed entropy value maps into a range of Jensen-Shannon complexity values and one can differentiate between regimes that are highly deterministic or highly stochastic and everything in-between. For more details on the permutation entropy and Jensen-Shannon complexity we refer to the reviews of Riedl et al. (2013) and Zanin et al. (2012).

3. Results

3.1. Choice of Chaotic and Stochastic Time Series

In this study we benchmark our results for geomagnetic indices with the Lorenz chaotic attractor (Ott, 2002):

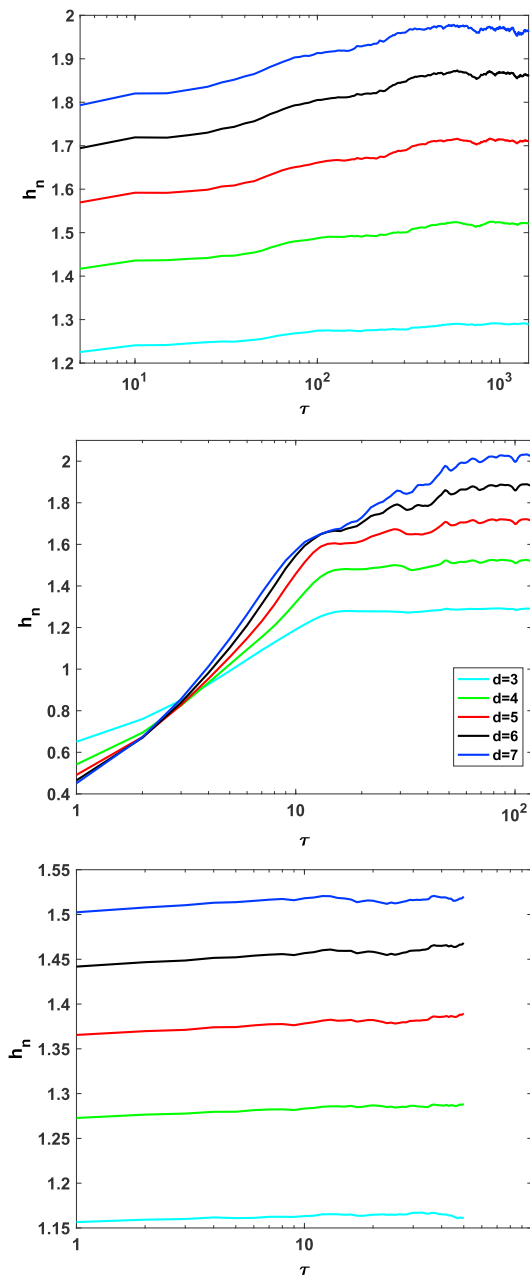


Figure 2. Permutation entropy as a function embedded delay τ and parametrized for embedding dimension $3 \leq d \leq 7$ for fractional Brownian motion with Hurst exponent $H = 0.75$ (top panel), the Lorenz attractor (center panel), and AL (bottom panel).

attractor, does not necessarily imply that AL is stochastic. Instead, it could indicate that a higher embedded dimension, that is, $d > 7$, is needed to samples all the patterns (Rosso et al., 2013). However, it is not always possible to pick $d > 7$, and we resort to the methodology of Rosso et al. (2007) to determine possible differences between AL and stochastic fluctuations.

3.3. Jensen-Shannon Complexity Plane

Before making use of the complexity-entropy plane, we first present the Jensen-Shannon complexity measure for AL as a function of embedded dimension and delay. The results are shown in Figure 3. The Jensen-Shannon complexity is computed against the embedded delay τ on the abscissa for all 12 months of the year 2010. The color represents the embedding dimension ranging between 3 and 6 with the same legend

$$\dot{X} = a(Y - X); \dot{Y} = X(c - Z) - Y; \dot{Z} = XY - bZ, \quad (6)$$

and fractional Brown motion (fBm) with Hurst exponent $h_u \in [0.01, 1]$ (Mandelbrot & Van Ness, 1968). We note that the choice of the Lorenz attractor rather than other well-known chaotic dynamical systems has no effect on our results. The reader can find a longer list of chaotic maps plotted in the complexity-entropy plane in reports by Rosso et al. (2007) and Maggs and Morales (2013) showing a clear demarcation between stochastic and chaotic time series. The parameters for the Lorenz attractor are $a = 10, b = 8/3, c = 28$. Figure 1 (top two panels) shows the time series for AL in black, and $\delta AL = AL_{j+1} - AL_j$ in magenta for 4-month time interval. Time series for the Lorenz strange attractor used for this study are shown as blue traces in Figure 1, and an example for the fBm with Hurst exponent $h_u = 0.8$ is shown on the bottom right panel of Figure 1 in red. The fBm is stochastic but can nonetheless be structured and contains trends (either persistent or antipersistent) and is used as the boundary delimiting stochastic and chaotic time series.

3.2. Permutation Entropy Analysis

In Figure 2, we plot the permutation entropy per symbol, h_n , for a stochastic, a chaotic and the AL time series as a function of embedded delay τ and embedded dimension $3 \leq d \leq 7$. Fractional Brownian motion with Hurst exponent of 0.75 is on the top panel. As with very other stochastic time series the permutation entropy is approximately constant across various τ and d . The small increase in the entropy is due to the fact that our choice of stochastic process has long autocorrelation times. Thus, for very long time delays, patterns become marginally more decorrelated.

In contrast, the center panel for the chaotic Lorenz attractor shows a minimum permutation entropy for $\tau = 1$. The permutation entropy then increases linearly with τ , until for sufficiently large delay of $\tau > 15$ the patterns become decorrelated. We also notice from the Lorenz attractor panel that for $\tau < 10$ the curves for $d = 7$ and $d = 6$ overlap. Hence, embedded dimension $d = 6$ is sufficient to track all the possible permutations for the Lorenz attractor. Or, put differently, increasing the embedded dimension to $d > 6$ does not provide more information about the complexity of the time series. Increasing the embedding dimension increases the range of patterns that are sampled in the time series. Thus, the result plotted for the Lorenz attractor is not surprising, since according to the well-known Takens' theorem (Ott, 2002), the embedded dimension must scale as $d = 2d_s + 1$ where d_s is the dimension of the strange attractor, which is well known to be between 2.03 and 2.06.

It is clear that the profile for AL , in the bottom panel, resembles the stochastic fractional Brownian motion with persistent increments. However, the absence of overlap for the various curves, as seen for the Lorenz

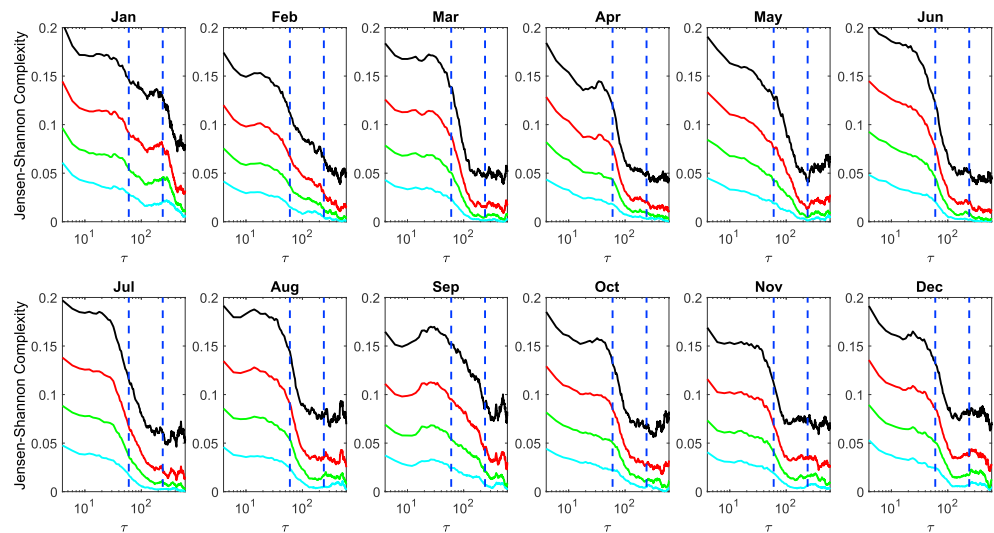


Figure 3. Jensen-Shannon complexity versus embedded delay τ for all 12 months of 2010 of AL values. The legend for the color is the same as in Figure 2. The embedded delay τ has units of minutes, and the dashed vertical lines indicate the 60- and 240-min marks.

as in Figure 2. Note that the complexity decreases for growing embedded delay. Hence, ordinal patterns are more correlated on small time scales ($\tau < 1$ hr) and become decorrelated for $\tau > 200$ – 240 min. Since the embedding dimension of AL is high, the complexity curves for $d = 6$ and $d = 5$ highlights local maximum and minimum that are missed by the $d = 4$ and $d = 3$ curve. For all months except May, June, July and November, we notice an enhancement in the complexity for $14 < \tau < 40$ and $d = 6$ after the initial monotonic decrease in complexity. A local maximum in complexity is particularly pronounced for the months of August and September. This indication of the presence of correlational structures with time scales ranging between 10 and 40 min is not a new result (Osmane et al., 2015) and will be discussed in the next section.

In Figure 4, we plot the complexity-entropy plane for $d = 6$, with minimum and maximum complexity-entropy curves in blue. The complexity-entropy points for fBm are plotted in red circles for $\tau = 1$ and Hurst exponents ranging between 0.01 and 1 by steps of 0.01. The points for fBm indicate a limit between stochastic and structured time series. The complexity-entropy values for the chaotic attractor are computed and plotted for the variable X , for $d = 6$ and $\tau = [1 - 10]$. The complexity values for the Lorentz attractor (cyan squares) have the smallest entropy for $\tau = 1$ and the largest for $\tau = 60$. We clearly see from Figure 4 that the complexity-entropy values for the Lorentz chaotic orbits skim the maximum curve; that is, for large entropies, the orbits of a chaotic attractor have large complexity values.

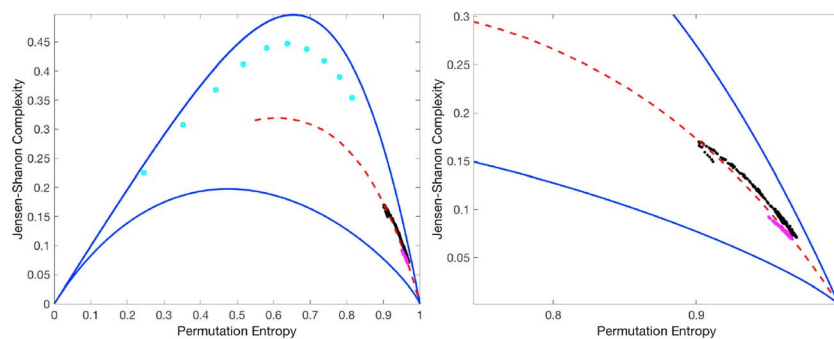


Figure 4. Complexity-entropy plane for AL (black dots), δAL (magenta dots), the Lorentz strange attractor (cyan squares), and fractional Brownian motion (red dash) on the left panel with a zoom in the low complexity high entropy part on the right panel. The blue curves represent the minimum and maximum entropy-complexity curve for an embedded parameter $d = 6$. The permutation entropy and Jensen-Shannon complexity values for AL and δAL are computed for $4 \leq \tau \leq 600$ min. The complexity values for AL reside along those for fractional-Brownian motion of Hurst exponents less than 0.5.

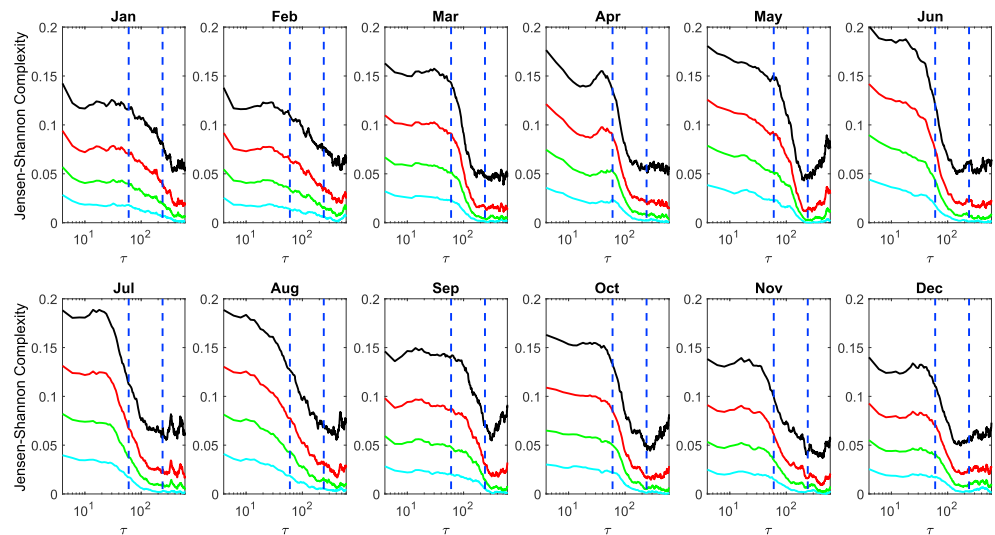


Figure 5. Jensen-Shannon complexity versus embedded delay τ for all 12 months of 2010 of AE values. The legend for the color is the same as in Figure 2.

Similarly, we plot on the same figure the complexity-entropy curve for both AL (black stars) and $\delta AL = \text{diff}(AL)$ (magenta dots) for $d = 6$ and time delay values ranging between $\tau = 4$ and $\tau = 600$ min by increments of 2 min. The lowest entropy values for AL and δAL are computed for $\tau = 4$, while the larger entropy values are for large $\tau > 500$. Figure 4 indicates that complexity-entropy values of AL overlap the fBm values for all subsampling parameters τ . As we increase τ , the entropy for AL increases, and the time series becomes indistinguishable from fractional Brownian motion with antipersistent increments, that is, with Hurst exponents less than 0.5.

It is natural to ask if the observed characterization of AL structures ranging between a few minutes to several hours is shared by other auroral current indices. In Figures 5 and 6, we show the dependence of the Jensen-Shannon complexity for all 12 months of 2010 for AE and AU , respectively. The range of parameters d , τ and the legend are the same as in Figure 3. Once again, the complexity value is relatively small for both indices. It peaks at low τ and decays for large τ values. Similarly to AL , we note that AE also experiences a local maximum in complexity values for embedded delay ranging between $\tau \approx 10$ and $\tau \approx 50$, albeit more pronounced and for different months (with the most obvious month being April). The complexity for AU on

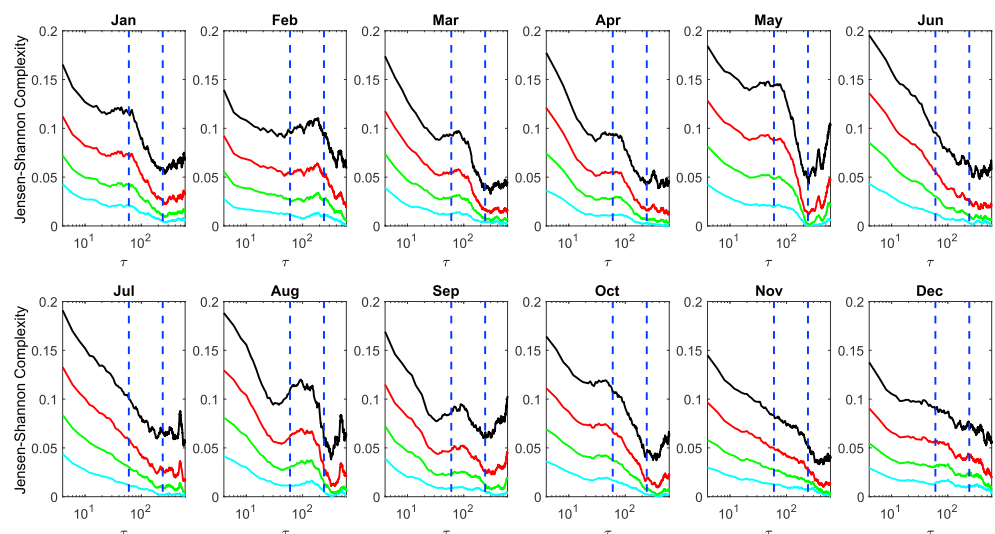


Figure 6. Jensen-Shannon complexity versus embedded delay τ for all 12 months of 2010 of AU values. The legend for the color is the same as in Figure 2.

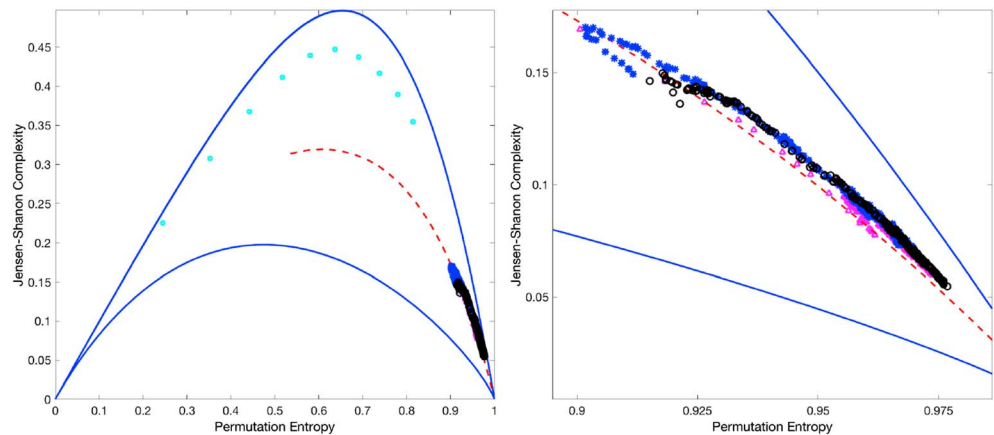


Figure 7. Complexity-entropy plane for *AL* (blue stars), *AU* (magenta lozenge), *AE* (black circles), and fractional Brownian motion (red dots) and $d = 6$. The lowest entropy values are computed for $\tau = 4$ min, while the larger entropy values are for $\tau = 600$ min. The complexity values for all three auroral geomagnetic indices reside along those for fractional-Brownian motion with Hurst exponents less than one half.

the other hand experiences local maximum for embedded delay ranging between $\tau \approx 30$ and $\tau \approx 200$ min, with the notable exception of June, July, and November where the complexity monotonically decreases until $\tau \approx 200$ and plateau at very low values thereafter. In Figure 7 we have reproduced the complexity-entropy plane for *AL* (blue stars) and fBm (red dots) and complemented it with values for *AE* (black circles) and *AU* (magenta lozenges) across the month of August 2010. Similarly as for *AL*, *AU*, and *AE* are highly stochastic across time scales ranging between a few minutes to 10 hr. We note that the same conclusion are equally valid for any other set of months (not shown).

4. Discussion and Conclusion

Using the permutation entropy developed by Bandt and Pompe (2002) and the complexity-entropy plane methodology developed by Rosso et al. (2007), we have demonstrated that geomagnetic indices have larger complexity (structures) and lower entropy (uncertainty) on small time scales of $\tau < 10$ than on time scales of $\tau > 10$ min. Nonetheless, auroral geomagnetic indices are indistinguishable from stochastic processes, overlapping with fractional Brownian processes on time scales ranging between a few minutes to 10 hr. Our results are therefore *inconsistent* with earlier studies of Baker et al. (1990), Pavlos et al. (1992), D. Roberts et al. (1991), D. A. Roberts (1991), and Vassiliadis et al. (1990, 1991) indicating that low-dimensional dynamical systems with chaotic properties might arise in geomagnetic current patterns.

In a similar study, Consolini and De Michelis (2014) also use permutation entropy as a measure of complexity to study the statistical properties of *SYM-H* time series spanning the period of January 2000 to December 2004. In their study, Consolini and De Michelis (2014) showed that permutation entropy computed on moving time windows was capable of capturing the rapid and local dynamical changes of *SYM-H*. During storms, intermittency and the nonstationary nature of the fluctuations of *SYM-H* was shown to correlate with lower permutation entropy and higher complexity during quiet times. This result is consistent with Figures 4 and 7 showing that for lower τ values, structures in auroral currents have higher complexity and lower entropy.

Following the work of Balasis et al. (2006), Consolini et al. (2013), and Osmane et al. (2015), our study also provides additional means to characterize large-scale and small-scale fluctuations originating in different physical processes. In a statistical study covering 17 years of OMNI data, Osmane et al. (2015) showed that probability distribution functions of *AL* responded in a nontrivial yet coherent fashion to various solar wind properties and ultralow frequency fluctuation amplitudes. For strongly southward interplanetary magnetic field (IMF), the *AL* distribution was characterized by a decrease of the skewness, a shift of the peak from -30 to -200 nT and a broadening of the distribution core. During northward IMF, the distribution in *AL* was instead characterized by a large reduction in the standard deviation and weight in the tail. Despite the different responses of the distribution function of *AL* for northward and southward IMF, the non-Gaussian changes were all occurring on time scales ranging between 10 and 40 min, similarly to the larger complexity

structures observed in *AL* and *AE* on comparable time scales (i.e., comparable τ values) and associated with intermittent fluctuations. In Osmane et al. (2015), the authors argued that the non-Gaussian properties in the Probability distribution function (Pdf) of *AL* occurring on time scales of the order of $\tau \sim 10\text{--}20$ min could be driven in part by viscous processes (Axford & Hines, 1961), such as Kelvin-Helmholtz instability (Nykyri & Otto, 2001) and kinetic Alfvén waves (Johnson & Cheng, 1997, 2001).

Whereas the mapping of auroral indices into the complexity-entropy plane was done independently of solar wind properties, follow-up studies could combine the methodology described in Osmane et al. (2015), and the one presented here to distinguish coherent geomagnetic responses to upstream solar wind conditions from internal magnetospheric dynamic processes. Future studies will be extended to other geomagnetic indices and focus particularly on different solar wind driving conditions that might explain the enhancement in complexity on small time scales of $\tau < 40$ min. Of particular interest, delineating storms in terms of solar wind conditions and statistics might indicate the contribution of magnetospheric dynamics in the triggering of storm activity and the nature of the nonlinear driving on time scales of minutes where viscous processes take place (Axford & Hines, 1961; Chaston et al., 2007; Freeman et al., 1968; Johnson & Cheng, 1997, 2001; Hasegawa et al., 2004, 2006; Lee et al., 1994; Nykyri & Otto, 2001; Nykyri et al., 2006), to hours where geomagnetic storms unfold (Pulkkinen, 2007).

Finally, it should be kept in mind that auroral geomagnetic indices do not necessarily account for the detailed spatial variations of the magnetic field. For instance, as the auroral electrojet expands in large storms, high-latitude observatories at which *AE* is derived experience lower magnetic field variations. Additionally, auroral geomagnetic indices cannot capture the complexity of the wider magnetospheric system since they are constructed as a multidimensional mapping of several observatories and reduced to a single proxy parameter. In the case of *AL*, it serves as a proxy for the energy transmitted into the ionosphere. We can therefore not exclude the possibility that spatial and/or temporal variations associated with various magnetospheric processes could be modeled in terms of a deterministic set of equations, albeit one that is not as low-dimensional as previous authors suggested. Rather, our analysis provides an answer to a much narrower question: Can we model fluctuations in auroral geomagnetic indices as low-dimensional chaotic attractors and consequently reduce a system a priori composed of a very large number degrees of freedom to one with a few degrees of freedom? Though our answer is undoubtedly in the negative, our analysis does not preclude the existence of a high-dimensional chaotic systems or one based on SOC models (Sharma et al., 2016).

Acknowledgments

This work was supported by Academy of Finland grants 267073/2013 and 297688/2015. A. O. would also like to thank James Weygand and Joe Borovsky for useful discussions on the use of the complexity-entropy approach to space data. The OMNI data used in this paper are available at the OMNI database (<http://omniweb.gsfc.nasa.gov>), free of charge.

References

- Axford, W. I., & Hines, C. O. (1961). A unifying theory of high-latitude geophysical phenomena and geomagnetic storms. *Canadian Journal of Physics*, 39, 1433.
- Baker, D., Klimas, A., McPherron, R., & Büchner, J. (1990). The evolution from weak to strong geomagnetic activity: An interpretation in terms of deterministic chaos. *Geophysical Research Letters*, 17(1), 41–44.
- Balasis, G., Daglis, I. A., Kapiris, P., Manda, M., Vassiliadis, D., & Eftaxias, K. (2006). From pre-storm activity to magnetic storms: A transition described in terms of fractal dynamics. *Annales Geophysicae*, 24, 3557–3567.
- Bandt, C., & Pompe, B. (2002). Permutation entropy: A natural complexity measure for time series. *Physical Review Letters*, 88(17), 174102.
- Berthelier, A., & Menvielle, M. (1993). Geomagnetic data 1987, IAGA indices: Aa, am, Kp, Dst, Ae, rapid variations. IAGA Bulletin, 32.
- Chang, T. (1992). Low-dimensional behavior and symmetry breaking of stochastic systems near criticality—can these effects be observed in space and in the laboratory? *IEEE Transactions on Plasma Science*, 20(6), 691–694.
- Chaston, C., Wilber, M., Mozer, F., Fujimoto, M., Goldstein, M., Acuna, M., et al. (2007). Mode conversion and anomalous transport in Kelvin-Helmholtz vortices and kinetic Alfvén waves at the Earth's magnetopause. *Physical Review Letters*, 99(17), 175004.
- Consolini, G., De Marco, R., & De Michelis, P. (2013). Intermittency and multifractal brownian character of geomagnetic time series. *Nonlinear Processes in Geophysics*, 20(4), 455–466.
- Consolini, G., & De Michelis, P. (2014). Permutation entropy analysis of complex magnetospheric dynamics. *Journal of Atmospheric and Solar-Terrestrial Physics*, 115, 25–31.
- Consolini, G., & Marcucci, M. (1997). Multifractal structure and intermittency in the AE index time series. *Nuovo cimento della Società italiana di fisica. C*, 20(6), 939–949.
- Dobias, P., & Wanliss, J. A. (2009). Intermittency of storms and substorms: Is it related to the critical behaviour? *Annales Geophysicae*, 27, 2011–2018.
- Farris, M. H., & Russell, C. T. (1994). Determining the standoff distance of the bow shock: Mach number dependence and use of models. *Journal of Geophysical Research*, 99, 17681.
- Freeman, J., Warren, C., & Maguire, J. (1968). Plasma flow directions at the magnetopause on January 13 and 14, 1967. *Journal of Geophysical Research*, 73(17), 5719–5731.
- Gollub, J. P., & Swinney, H. L. (1975). Onset of turbulence in a rotating fluid. *Physical Review Letters*, 35(14), 927.
- Grassberger, P., & Procaccia, I. (1983). Characterization of strange attractors. *Physical Review Letters*, 50(5), 346.
- Hasegawa, H., Fujimoto, M., Phan, T.-D., Reme, H., Balogh, A., Dunlop, M., et al. (2004). Transport of solar wind into Earth's magnetosphere through rolled-up Kelvin-Helmholtz vortices. *Nature*, 430(7001), 755–758.

- Hasegawa, H., Fujimoto, M., Takagi, K., Saito, Y., Mukai, T., & Rème, H (2006). Single-spacecraft detection of rolled-up Kelvin-Helmholtz vortices at the flank magnetopause. *Journal of Geophysical Research*, *111*, A09203. <https://doi.org/10.1029/2006JA011728>
- Johnson, J. R., & Cheng, C. Z. (1997). Kinetic Alfvén waves and plasma transport at the magnetopause. *Geophysical Research Letters*, *24*, 1423–1426.
- Johnson, J. R., & Cheng, C. Z. (2001). Stochastic ion heating at the magnetopause due to kinetic Alfvén waves. *Geophysical Research Letters*, *28*, 4421–4424.
- King, J. H., & Papitashvili, N. E. (2005). Solar wind spatial scales in and comparisons of hourly Wind and ACE plasma and magnetic field data. *Journal of Geophysical Research*, *110*, A02104. <https://doi.org/10.1029/2004JA010649>
- Klimas, A. J., Valdivia, J. A., Vassiliadis, D., Baker, D. N., Hesse, M., & Takalo, J. (2000). Self-organized criticality in the substorm phenomenon and its relation to localised reconnection in the magnetospheric plasma sheet. *Journal of Geophysical Research*, *105*, 18,765–18,780.
- Klimas, A. J., Vassiliadis, D., Baker, D. N., & Roberts, D. A. (1996). The organized nonlinear dynamics of the magnetosphere. *Journal of Geophysical Research*, *101*, 13,089–13,114.
- Landau, L. D. (1944). On the problem of turbulence. *Dokl. akad. nauk sssr*, *44*, 339–349.
- Lee, L., Johnson, J. R., & Ma, Z. (1994). Kinetic alfvén waves as a source of plasma transport at the dayside magnetopause. *Journal of Geophysical Research*, *99*(A9), 17,405–17,411.
- Lovejoy, S., & Schertzer, D. (1998). Stochastic chaos and multifractal geophysics. *Chaos, Fractals and Models*, *96*, 38–52.
- Maggs, J., & Morales, G. (2013). Permutation entropy analysis of temperature fluctuations from a basic electron heat transport experiment. *Plasma Physics and Controlled Fusion*, *55*(8), 85015.
- Mandelbrot, B. B., & Van Ness, J. W. (1968). Fractional Brownian motions, fractional noises and applications. *SIAM Review*, *10*(4), 422–437.
- Newell, P., Sotirelis, T., Liou, K., Meng, C.-I., & Rich, F. (2007). A nearly universal solar wind-magnetosphere coupling function inferred from 10 magnetospheric state variables. *Journal of Geophysical Research*, *112*, A01206. <https://doi.org/10.1029/2006JA012015>
- Nykyri, K., & Otto, A. (2001). Plasma transport at the magnetospheric boundary due to reconnection in Kelvin-Helmholtz vortices. *Geophysical Research Letters*, *28*(18), 3565–3568.
- Nykyri, K., Otto, A., Lavraud, B., Mouikis, C., Kistler, L. M., Balogh, A., & Rème, H. (2006). Cluster observations of reconnection due to the Kelvin-Helmholtz instability at the dawnside magnetospheric flank. *Annales Geophysicae*, *24*, 2619–2643.
- Osborne, A. R., & Provenzale, A. (1989). Finite correlation dimension for stochastic systems with power-law spectra. *Physica D: Nonlinear Phenomena*, *35*(3), 357–381.
- Osmane, A., Dimmock, A., Naderpour, R., Pulkkinen, T., & Nykyri, N. (2015). The impact of solar wind ULF b_z fluctuations on geomagnetic activity for viscous timescales during strongly northward and southward IMF. *Journal of Geophysical Research: Space Physics*, *120*, 9307–9322. <https://doi.org/10.1002/2015JA021505>
- Ott, E. (2002). *Chaos in dynamical systems*. Cambridge, UK: Cambridge University Press.
- Pavlos, G., Kyriakou, G., Rigas, A., Liatsis, P., Trochoutsos, P., & Tsonis, A. (1992). Evidence for strange attractor structures in space plasmas. *In Annales Geophysicae*, *10*, 309–322.
- Prichard, D., & Price, C. (1992). Spurious dimension estimates from time series of geomagnetic indices. *Geophysical Research Letters*, *19*(15), 1623–1626.
- Pulkkinen, T. (2007). Space weather: Terrestrial perspective. *Living Reviews in Solar Physics*, *4*(1), 60.
- Pulkkinen, A., Klimas, A., Vassiliadis, D., & Uritsky, V. (2006). Role of stochastic fluctuations in the magnetosphere-ionosphere system: A stochastic model for the AE index variations. *Journal of Geophysical Research*, *111*, A10218. <https://doi.org/10.1029/2006JA011661>
- Riedl, M., Muller, A., & Wessel, N. (2013). Practical considerations of permutation entropy. *The European Physical Journal Special Topics*, *222*, 249.
- Roberts, D. A. (1991). Is there a strange attractor in the magnetosphere? *Journal of Geophysical Research*, *96*(A9), 16,031–16,046.
- Roberts, D., Baker, D., Klimas, A., & Bargatze, L. (1991). Indications of low dimensionality in magnetospheric dynamics. *Geophysical Research Letters*, *18*(2), 151–154.
- Rosso, O. A., Larrondo, H. A., Martin, M. T., Plastino, A., & Fuentes, M. A. (2007). Distinguishing noise from chaos. *Physical Review Letters*, *99*(15), 154102.
- Rosso, O. A., Olivares, F., Zunino, L., De Micco, L., Aquino, A. L. L., Plastino, A., & Larrondo, H. A. (2013). Characterization of chaotic maps using the permutation Bandt-Pompe probability distribution. *European Physical Journal B*, *86*, 116.
- Ruelle, D., & Takens, F. (1971). On the nature of turbulence. *Communications in Mathematical Physics*, *20*(3), 167–192.
- Shan, L.-H., Hansen, P., Goertz, C., & Smith, R. (1991). Chaotic appearance of the AE index. *Geophysical Research Letters*, *18*(2), 147–150.
- Sharma, A. S., Aschwanden, M. J., Crosby, N. B., Klimas, A. J., Milovanov, A. V., Morales, L., et al. (2016). 25 years of self-organized criticality: Space and laboratory plasmas. *Space Science Reviews*, *198*, 167–216.
- Takalo, J., Timonen, J., & Koskinen, H. (1994). Properties of AE data and bicolored noise. *Journal of Geophysical Research*, *99*(A7), 13,239–13,249.
- Tanskanen, E., Pulkkinen, T., Koskinen, H., & Slavin, J. (2002). Substorm energy budget during low and high solar activity: 1997 and 1999 compared. *Journal of Geophysical Research*, *107*(A6), 1086.
- Uritsky, V. M., Klimas, A. J., & Vassiliadis, D. (2006). Analysis and prediction of high-latitude geomagnetic disturbances based on a self-organized criticality framework. *Advances in Space Research*, *37*(3), 539–546.
- Uritsky, V. M., & Pudovkin, M. I. (1998). Low frequency 1/f-like fluctuations of the AE-index as a possible manifestation of self-organized criticality in the magnetosphere. *Annales Geophysicae*, *16*, 1580–1588.
- Uritsky, V., Pudovkin, M., & Steen, A. (2001). Geomagnetic substorms as perturbed self-organized critical dynamics of the magnetosphere. *Journal of Atmospheric and Solar-Terrestrial Physics*, *63*(13), 1415–1424.
- Valdivia, J., Klimas, A., Vassiliadis, D., Uritsky, V., & Takalo, J. (2003). Self-organization in a current sheet model, *Advances in space environment research* (pp. 515–522): Springer.
- Vassiliadis, D. V., Sharma, A. S., Eastman, T. E., & Papadopoulos, K. (1990). Low-dimensional chaos in magnetospheric activity from AE time series. *Geophysical Research Letters*, *17*, 1841–1844.
- Vassiliadis, D., Sharma, A., & Papadopoulos, K. (1991). Lyapunov exponent of magnetospheric activity from AL time series. *Geophysical Research Letters*, *18*(8), 1643–1646.
- Wanliss, J. A., Anh, V. V., Yu, Z.-G., & Watson, S. (2005). Multifractal modeling of magnetic storms via symbolic dynamics analysis. *Journal of Geophysical Research*, *110*, A08214. <https://doi.org/10.1029/2004JA010996>
- Wanliss, J. A., & Dobias, P. (2007). Space storm as a phase transition. *Journal of Atmospheric and Solar-Terrestrial Physics*, *69*, 675–684.
- Weck, P. J., Schaffner, D. A., Brown, M. R., & Wicks, R. T. (2015). Permutation entropy and statistical complexity analysis of turbulence in laboratory plasmas and the solar wind. *Physical Review E*, *91*(2), 23101. <https://doi.org/10.1103/PhysRevE.91.023101>

Zanin, M., Zunino, L., Rosso, O. A., & Papo, D. (2012). Permutation entropy and its main biomedical and econophysics applications: A review. *Entropy*, *14*, 1553–1577.